Vol. 17, No. 1 (2018) 215-228
Revista Mexicana de Ingeniería Química

PREPARATION AND EVALUATION OF NiCoMo HYDRODESULFURIZATION CATALYSTS SUPPORTED OVER A BINARY ZEOLITE(BETA)-KIT-6 SILICEOUS MATERIAL

PREPARACIÓN Y EVALUACIÓN DE CATALIZADORES NiCoMo PARA HIDRODEZULFURIZACIÓN SOPORTADOS SOBRE UN MATERIAL DE SILICIO BINARIO ZEOLITA(BETA)-KIT-6

G. Torres-Otáñez[1], J.N. Díaz-de León[1]*, T.A. Zepeda[1], B. Pawelec[2], J.L.G. Fierro[2], S. Fuentes[1]
[1]*Universidad Nacional Autónoma de México, Centro de Nanociencias y Nanotecnología. Km. 107 Carretera Tijuana-Ensenada, Ensenada, B.C. CP 22860.*
[2]*Instituto de Catálisis y Petroleoquímica, CSIC, Marie Curie 2, Cantoblanco, 28049 Madrid, Spain.*
Received June 8, 2017; Accepted July 26, 2017

Abstract
In this work, a mesoporous nanocomposite Zeolite(Beta)-KIT-6 material was synthesized and used as a support to prepare NiCoMo catalysts. We prepared CoMo, NiMo (Co or Ni =2.4 wt.% and Mo=9.0 wt%) and (x)NiCoMo (x = 0.6, 1.2, and 2.4 wt% Ni). The support and catalysts were characterized and tested in the hydrodesulfurization (HDS) reaction of dibenzothiophene (DBT). The catalytic activity results show that the CoMo and NiMo samples are more active than the trimetallic catalysts due to a better dispersion of MoS_2 (lower stacking and length) which induce a higher concentration of CoMoS and NiMoS sites. The HRTEM results also showed that the increase of the Ni concentration causes the increase of length and stacking of the MoS_2 slabs. The XPS analysis exhibited that the amount of Co sulfided species in trimetallic catalysts follows a linear trend with the catalytic activity. The β-KIT-6 bimetallic supported catalysts showed better catalytic activities than those supported on KIT-6 and SBA-15 mesoporous silicas.
Keywords: KIT-6, NiMo, CoMo, hydrodesulfurization, zeolite.

Resumen
En este trabajo, un material mesoporoso Zeolita (Beta)-KIT-6 fue sintetizado y usado como soporte para preparar catalizadores NiCoMo. Preparamos catalizadores CoMo, NiMo (Co o Ni = 2.4 % en peso y Mo = 9.0 % en peso) y (x)NiCoMo (x = 0.6, 1.2 y 2.4 % en peso de Ni). El soporte y los catalizadores fueron caracterizados y evaluados en la reacción de hidrodesulfurización (HDS) de dibenzotiofeno (DBT). Los resultados de la actividad catalítica muestran que las muestras de CoMo y NiMo son más activas que los catalizadores trimetálicos debido a una mejor dispersión de MoS_2 (bajo apilamiento y longitud) la cual induce a una más alta concentración de sitios CoMoS y NiMoS. Los resultados de HRTEM además muestran que el incremento de la concentración de Ni causa el incremento en la longitud y el apilamiento de las laminillas de MoS_2. El análisis de XPS mostró que la cantidad de especies de Co sulfurado en los catalizadores trimetálicos seguían una tendencia lineal con la actividad catalítica. Los catalizadores bimetálicos soportados en β-KIT-6 mostraron mejores actividades catalíticas que los soportados sobre silicas mesoporosas KIT-6 y SBA-15.
Palabras clave: KIT-6, NiMo, CoMo, hidrodesulfuración, zeolita.

1 Introduction

The sulfur oxide compounds of exhaust emissions from gasoline and diesel fuels combustion processes are very harmful air pollutants to human health and the environment. Therefore, sulfur must be removed from the fuels during refining before arriving at transportation systems. Hence, due to environmental protection, the fuel S content has to be limited near to zero on fuel specifications (Song *et al*., 2003; Zhang *et al*., 2010). Various methods to remove S in oil distillates have been proposed in many developed countries, such as hydrogenation, adsorption, biological desulfurization, however, among these technologies, the most effective process for large scale industrial production is the

* *Corresponding author. E-mail*: noejd@cnyn.unam.mx
doi: 10.24275/uam/izt/dcbi/revmexingquim/2018v17n1/Torres
issn-e: 2395-8472

catalytic hydrotreating (Trejo *et al*., 2008).

To reach very low sulfur levels in traditional fuels, hydrotreating processes using severe conditions have to be applied, but to maintain the industrial economy, highly active catalysts are required. The industrial catalyst employed in this type of processes are MoS_2-based and supported on alumina. In particular, the addition of Co or Ni allows the formation of non-stoichiometric CoMoS or NiMoS active phases for hydrodesulfurization (HDS) and are widely described in the literature (Topsoe *et al*., 1996).

It is well known that support plays an important role in the performance of HDS catalysts, including loading and dispersing of the active component (Gutierrez *et al*., 2014). Numerous efforts have been made to evaluate and improve the catalytic performance of hydrodesulfurization catalysts by changing the standard support i.e. SBA-15 (Suresh *et al*., 2017; Gutierrez *et al*., 2006), HMS (Zepeda *et al*., 2014), ZrO_2 (Kaluz *et al*., 2012), TiO_2 (Guo *et al*., 2013), Al_2O_3 (Munguía-Guillen *et al*., 2016) and MgO (Pratt *et al*., 1990). As well several studies have been published on mixed oxides for HDS catalysts, e.g. Al_2O_3-TiO_2 (Tavizón-Pozos *et al*., 2016; Ramirez *et al*., 1993; Olguín *et al*., 1997), TiO_2-SiO_2 (Reddy *et al*., 2001), TiO_2-ZrO_2 (Escobar *et al*., 2013), among others. Recently, our research group published the use of KIT-6 siliceous material doped with Al as support of CoMo catalysts (Suresh *et al*., 2017). These Al-KIT-6 materials were very suitable to prepare efficient HDS catalysts. The CoMo/Al KIT-6 catalysts showed a highly active behavior in the HDS of dibenzothiophene.

In this work, we focus our research on the preparation of a binary Zeolite(beta)-KIT-6 material (β-KIT-6) to be used as support for trimetallic (x)NiCoMo HDS catalysts. A series of CoMo, NiMo, and (x)NiCoMo catalysts were prepared by co-impregnation with x being the increasing weight % (wt%) content of Ni (x = 0.6,1.2, 2.4 wt%). In these samples the Co and Mo content was kept constant, Co = 2.4 wt% and Mo=9.0 wt%. The samples were characterized by X-ray diffraction (XRD), N_2 physisorption and high-resolution transmission electron microscopy (HRTEM). The oxide catalysts were characterized by DRX and N_2 physisorption. Meanwhile, the sulfided catalysts were characterized by HRTEM and X-ray photoelectron spectroscopy (XPS). Finally, the catalytic activity was tested in the HDS of DBT in a batch reactor under a high pressure of hydrogen.

2 Experimental

2.1 Preparation of the support

Support β-KIT-6 was prepared using a three step synthesis method modified from a previous report (Zhang *et al*., 2010). A zeolite seed solution was prepared by adding 0.2 g of NaOH, 0.76 g of $NaAlO_2$, and 21.4 g of tetraethylorthosilicate (TEOS) into 31.5 g of an aqueous solution of tetraethyl ammonium hydroxide (TEAOH 25% vol). The mixture was stirred for 4 h at room temperature and then transferred into an autoclave for aging at 140 °C for 36 h to obtain a zeolite Beta seed solution. An amount of 2 g of $EO_{20}PO_{70}EO_{20}$ (Pluronic P123) was dissolved in 49 g of H_2O with 27 g of 2 M hydrochloric acid at 35 °C and 2.9 g of *n*-butanol were added to the mixture and stirred for 3 h. Finally, 6 g of TEOS and 10 g of zeolite seed solution were mixed with the P123 solution. The mixture was stirred for 24 h at 35 °C and then transferred to an autoclave for further reaction at 100 °C for 24 h. The aluminosilicate precursor was collected by filtration, dried at 100 °C for 12 h, and calcined at 550 °C in air for 6 h with a heating rate of 1 °C min^{-1} to remove the template.

2.2 Catalyst preparation

The calcined support was impregnated by the pore-filling method with solutions containing the CoMo and NiCoMo precursors and citric acid (CA) as an organic additive. The loadings were 0.6, 1.2 and 2.4 wt.% for Ni, 2.4 wt.% for Co and 9.0 wt.% for Mo. The catalysts were obtained by simultaneous impregnation of ammonium heptamolybdate ($(NH_4)_6Mo_7O_{24}$), cobalt nitrate $Co(NO_3)_2{\cdot}6H_2O$ and nickel nitrate $Ni(NO_3)_2{\cdot}6H_2O$. First, CA was dissolved under stirring in ammonium hydroxide solution, then $(NH_4)_6Mo_7O_24$ was added into the CA solution. Finally, cobalt nitrate was dissolved, and the support was impregnated having a pH of 3.5 for the bimetallics catalysts. For trimetallic catalysts NiCoMo the nickel nitrate was dissolved after the cobalt nitrate giving a pH of 4 for trimetallics catalysts. The Co/CA molar ratio was equal to 1. The samples were dried at 120 °C for 12 h, and calcined at 450 °C in air for 4 h.

2.3 Physicochemical characterization techniques

The textural properties of the materials were determined by N_2 adsorption-desorption isotherms on a TriStar II 3020 Micromeritics equipment. Before the experiments, the materials were degassed at 250 °C in vacuum for 5 h. The volume of the adsorbed N_2 was normalized to the standard temperature and pressure. The surface areas (S_{BET}) were calculated by the BET equation applied to the range of relative pressures $0.05 < P/P_0 < 0.30$. The average pore diameter was calculated by applying the Barret-Joyner-Halenda method (BJH) to the adsorption branches of the N_2 isotherms. The cumulative pore volume was obtained from the isotherms at $P/P_0 = 0.97$.

The X-ray diffraction (XRD) patterns of the samples were registered it in a Philips spectrometer model X'pert using the Cu Kα radiation (40 kV, 30 mA) with a wavelength of 0.154 nm. X-ray photoelectron spectra (XPS) of the calcined and fresh sulfided catalysts were recorded on an ESCALAB 200R electron spectrometer equipped with a hemispherical electron analyzer, using an Mg Kα (hν = 1253.6 eV, 1 eV = 1.6032 $\times 10^{-19}$J) X-ray source. The catalysts were sulfided *ex-situ* in a flowing H_2S:H_2 mixture (1:10) at 400 °C for 1 h. After sulfidation, the catalysts were kept under i-octane to avoid exposure to air and then transferred to the ion-pumped XPS analysis chamber. The introduction of the sulfided samples to the XPS analysis chamber was carried out under argon atmosphere conditions to avoid air contact.

The substrate morphology was analyzed by scanning electron microscopy (SEM) using a JEOL JSM-5300. HRTEM micrographs were collected on a JEOL JEM-2100F instrument. The samples were suspended in isopropyl alcohol as a solvent to be deposited on Cu grid.

2.4 Catalytic activity measurements

Before the HDS reaction, the samples were ex-situ sulfided under a 15 vol% H_2S/H_2 flow (40 mL min^{-1}) at 400 °C with a heating rate of 5 °C min^{-1} for 1 h. Then, they were introduced in a 500 mL batch reactor with the reactants. The conditions of the tests were as follows: temperature, 320 °C, a hydrogen atmosphere, 800 psi (5.5 MPa), sulfided catalyst 0.25 g and DBT concentration, 0.22 g dissolved in 100 mL of hexadecane. Reaction products were periodically collected for 5 h and analyzed quantitatively by gas chromatography. The catalytic activity was expressed by the initial reaction rate (mol$_{DBT}$ g$_{cat}^{-1}$s^{-1}).

3 Results

3.1 Support characterization

The β-KIT-6 synthesized material calcined at 500°C was characterized to verify their textural and physicochemical properties. The N_2 physisorption isotherm and the pore size distribution obtained for the β-KIT-6 sample is displayed in Fig. 1.

The Fig. 1A present the adsorption-desorption isotherm for the β-KIT-6 sample, which resulted of a type IV isotherm with a hysteresis loop H1 type (Thommes *et al.*, 2015). The capillarity condensation point was observed at relative pressure 0.45. The specific surface area was 807 m^2 g^{-1} (BET), the pore volume (P_v) 0.65 and the average pore size resulted of 39.9 Å (P_z).

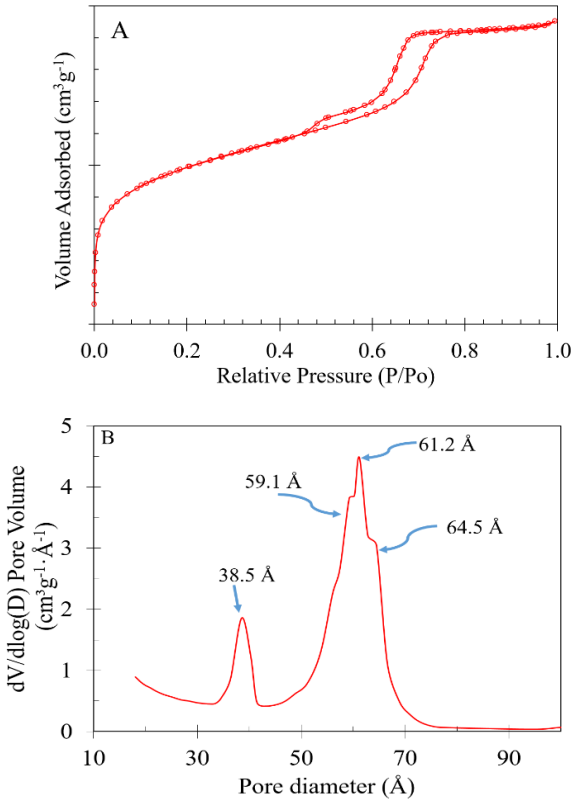

Fig. 1. N_2 Adsorption-desorption isotherm (A) and pore size distribution (B) for the calcined β-KIT-6 sample.

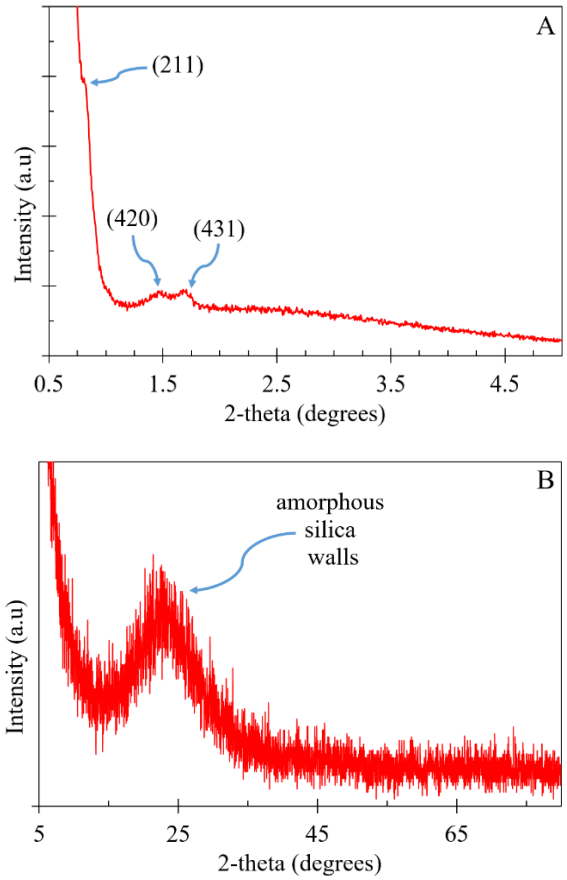

Fig. 2 Small (A) and wide (B) angle XRD patterns for the calcined β-KIT-6 sample.

From the pore size distribution shown in Fig. 1B, it is possible to observe that the pore size distribution presented two main peaks; the first one centered at 38.5 Å and the second one centered approximately at 61.2 Å. In the second distribution, two shoulders were observed, the first one around 59.1 Å and the second one at 64.5 Å. This pore size distribution is related to the presence of internal pore 3D structure (Kim *et al*., 2015).

The small and wide-angle XRD patterns for the β-KIT-6 are shown in Fig. 2. In Fig. 2A the peaks at 0.98°, 1.70° and 1.96° corresponded to planes (211), (420) and (431), respectively. These are typical Bragg reflections reported for KIT-6 samples (Rezaei *et al*., 2017). The Fig. 2B displayed an amorphous diffraction pattern with a broad diffraction peak around 20-30° degrees, which is related to the amorphous β-KIT-6 wall of the mesoporous material (He *et al*., 2016).

The morphology of β-KIT-6 support was investigated by HRTEM. In Fig. 3 several zones of well-ordered cubic 3D mesoporous channels are

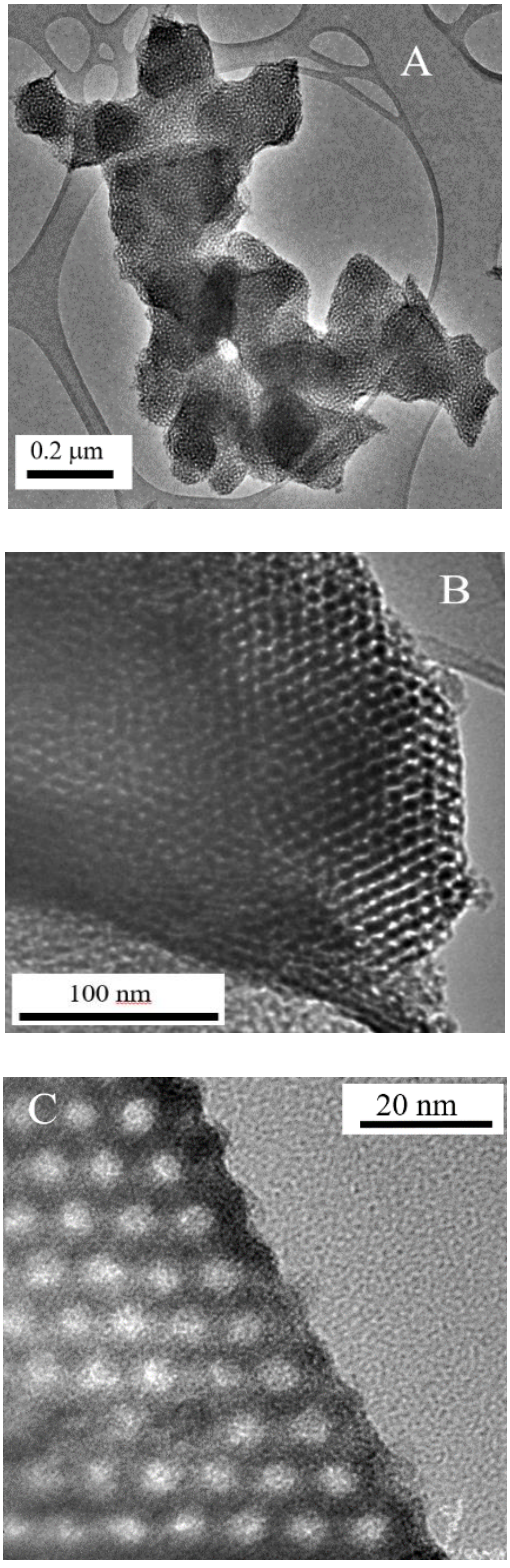

Fig. 3 General view of HRTEM micrographs for the calcined β-KIT-6 support.

distinguished at different magnifications. In Fig. 3A at low magnification the general porous structure is observed with the cubic structure (Ia3d). The micrograph in Fig. 3B at medium magnification presents a regular pore distribution with a pore width around 39.5 Å; which corresponds with the first unimodal distribution centered at 38.5 Å, similar to the pore size distribution exhibited in Fig. 1B. Also in this picture, several holes seem to be containing material that could be the zeolite beta. The magnified image in Fig. 3C shows that pores are distributed in a hexagonal arrangement as expected for KIT-6 material.

3.2 *Oxide catalysts characterization*

3.2.1 *N_2 adsorption-desorption isotherms*

The N_2 adsorption-desorption isotherms and the pore size distribution calculated by the BJH method for the catalysts are presented in Fig. 4. As seen in Fig. 4A all materials showed similar physisorption isotherms type IV according to IUPAC classification (Thommes *et al*. (2015)) and corresponded to mesoporous adsorbents with H1-type hysteresis loop. It has been reported for the KIT-6 (Suresh *et al*. (2017)) (Wei *et al*. (2017)) that it exhibits a narrow range of uniform ordered mesoporous (Gao *et al*. (2015)). The presence of this kind of hysteresis is characteristic of cylindrical pores (Gotier *et al*. (1995)) (Zepeda *et al*. (2005)), as other siliceous materials i.e. MCM-41(Abrokwah *et al*. (2016)), MCM-48(Souza *et al*. (2015)) and SBA-15(Alonso-Núñez *et al*. (2012)). After impregnation of Ni, Co, and Mo metal oxide species on the *β*-KIT-6 support, no significant changes were observed in the characteristic shape of the isotherms. This confirms that the original pore structure of the support was preserved in the trimetallic catalysts. However, a significant decrease in the quantity of nitrogen adsorbed was observed after metal deposition for all (x)NiCoMo catalysts.

The textural properties of porous materials, such as surface area, pore volume and the average pore size calculated by the BJH method are listed in Table 1. The specific area gradually decreased with the increase of the Ni concentration as compared with the *β*-KIT-6 support. The surface area trend resulted as follows: NiMo/*β*-KIT-6 > CoMo/*β*-KIT-6 > 2.4NiCoMo/*β*-KIT-6 > 1.2NiCoMo/*β*-KIT-6 > 0.6NiCoMo/*β*-KIT-6. The observed decrease for the CoMo/*β*-KIT-6 and NiMo/*β*-KIT-6 samples was about 60% compared to the *β*-KIT-6 support surface area. For the trimetallic (x)NiCoMo/*β*-KIT-6 systems the

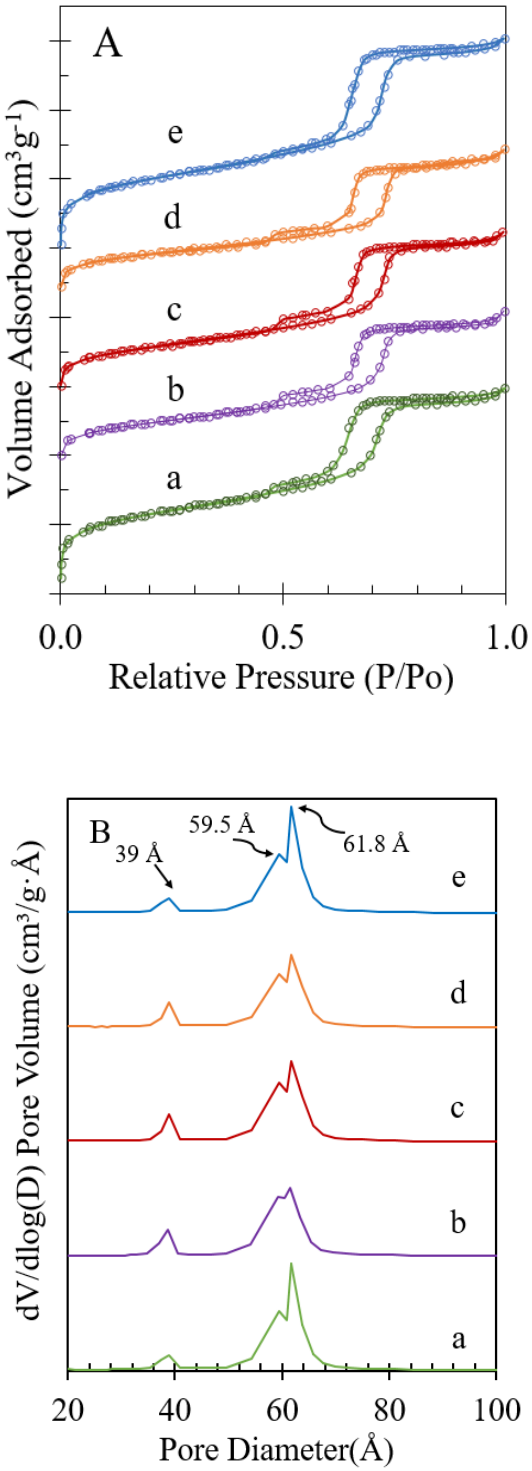

Fig. 4. A) Nitrogen adsorption/desorption isotherms, B) Pore size distribution for a) CoMo/*β*-KIT-6, b) 0.6NiCoMo/*β*-KIT-6, c) 1.2NiCoMo/*β*-KIT-6, d) 2.4NiCoMo/*β*-KIT-6, and e) NiMo/*β*-KIT-6 catalysts.

Table 1. Textural properties of (x)NiCoMo/β-KIT-6 catalysts.

Samples β-KIT-6	S^a_{BET} (m^2 g^{-1})	V^b_t(cm^3 g^{-1})	d^c_{BJH} (nm)
CoMo	300	0.4	5.5
0.6NiCoMo	235	0.33	5.5
1.2NiCoMo	265	0.36	5.4
2.4NiCoMo	272	0.34	5.6
NiMo	325	0.42	5.3

[a]BET method. [b]at a relative pressure of 0.98. [c]BJH method.

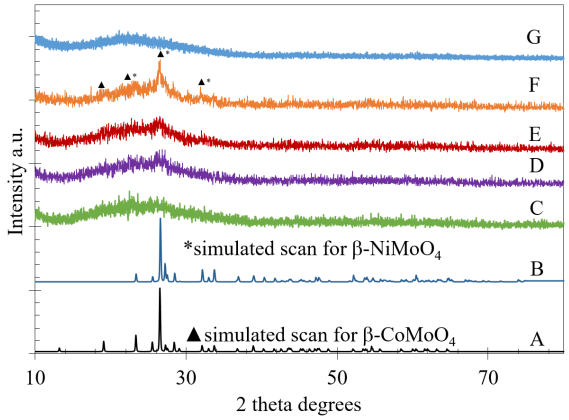

Fig. 5 XRD patterns for A) β-$CoMoO_4$ simulated scan B) β-$NiMoO_4$, C) CoMo/β-KIT-6, D)0.6NiCoMo/β-KIT-6, E) 1.2NiCoMo/β-KIT-6, F) 2.4NiCoMo/β-KIT-6, and G) NiMo/β-KIT-6 catalysts.

surface area was only 7% lower than for the NiMo and CoMo bimetallic catalysts.

We can observe in Fig. 4B that the main peak centered at 61.8 Å in the pore size distribution decreased with the presence of the impregnated metal oxides, although, the bimodal pore size distribution was still observed, as in the support profile.

3.2.2 XRD

The XRD patterns of the calcined catalysts are presented in Fig. 5. In general, all XRD patterns of the catalysts displayed a broad diffraction related to the amorphous silica walls between 20-30°. Nevertheless, in the CoMo/β-KIT-6 sample (Fig. 5C) a small wide shoulder appeared around 26.4°, with the incorporation of Ni in the samples (0.6, 1.2 and 2.4 wt%), see Fig. 5D to 5E, respectively. Other peaks at 23.3° and 19.1° start to be noticed at high Ni concentration. The presence of these peaks may be related to the formation of β-$CoMoO_4$ (Fig.5A) or β-$NiMoO_4$ (Fig. 5B) oxide crystalline phases (PDF-21-868 and PDF-45-142 respectively) after a calcination thermal treatment at 350°C (Gonzales-Cortés *et al.*, 2015). It seems that the excess of Ni inhibits the formation of trimetallic citrate species during the impregnation step, forming β-$CoMoO_4$ segregated phase which is stable and more difficult to sulfurize than $NiMoO_4$ (Gonzales-Cortés *et al.*, 2006).

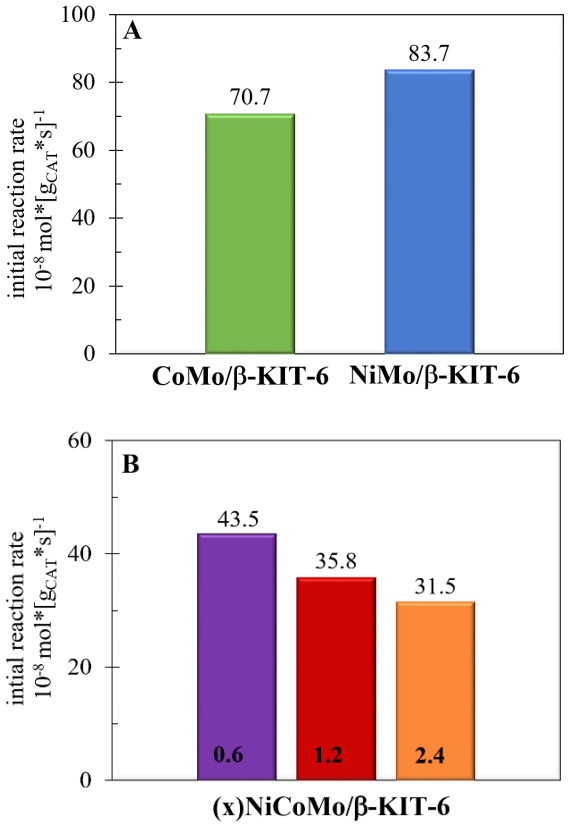

Fig. 6. Initial reaction rate for A) CoMo/β-KIT-6 and NiMo/β-KIT-6, B) (x)NiCoMo/β-KIT-6.

3.3 Sulfided catalysts characterization

3.3.1 Catalytic test

The catalytic activity of the catalysts was tested in the hydrodesulfurization of dibenzothiophene, P=800 psi and T=320°C. The initial reaction rates for all pre-sulfided catalyst are shown in Fig. 6.

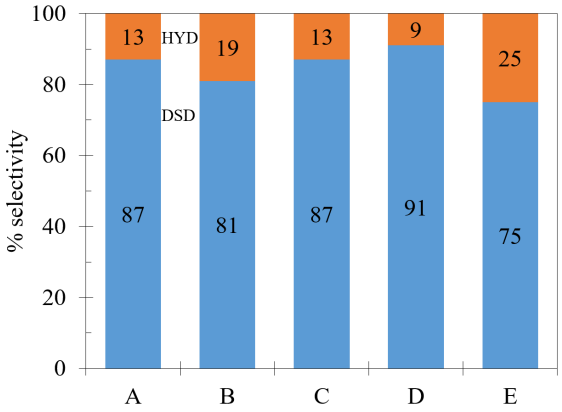

Fig. 7. Selectivity values obtained at 30% conversion for the A) CoMo/β-KIT-6, B)0.6NiCoMo/β-KIT-6, C)1.2NiCoMo/β-KIT-6, D)2.4NiCoMo/β-KIT-6, and E) NiMo/β-KIT-6 sulfided catalysts.

The Fig. 6A presents the activities for the CoMo and NiMo bimetallic catalysts prepared on the β-KIT-6 sample. The catalytic activity of CoMo/β-KIT-6 sample was 70.7 $\times 10^{-8}$ mol_{DBT} $g_{cat}^{-1}s^{-1}$, this value was 2.5 times higher than that obtained previously for a reference $CoMo/Al_2O_3$ (28 $\times 10^{-8}$ mol_{DBT} $g_{cat}^{-1}s^{-1}$) catalyst evaluated under the same reaction conditions (Suresh *et al*. (2017)). Also, this material exhibited 12% more activity than the CoMo/KIT-6 (28 $\times 10^{-8}$ mol_{DBT} $g_{cat}^{-1}s^{-1}$) and 2.3 times higher than the CoMo catalyst supported on SBA-15 (30.5 $\times 10^{-8}$ mol_{DBT} $g_{cat}^{-1}s^{-1}$) (Suresh *et al*., 2017). In the case of the NiMo/β-KIT-6, the catalyst activity was 83.7 $\times 10^{-8}$ mol_{DBT} $g_{cat}^{-1}s^{-1}$ which was 18 % higher than the CoMo/β-KIT-6. Such a difference in activity between CoMo and NiMo is typical of these systems. The Fig. 6B shows the effect of Ni incorporation into the CoMo system. Unexpectedly, the catalytic activity decreased with the Ni presence in the catalysts formulation. With only 0.6 Ni wt.% the activity loss was of around 39% compared with the CoMo/β-KIT-6 catalysts. The addition of 1.2wt% Ni induced a lost near to 50% and further increase on the Ni content (2.4 wt%) led to a decrease in activity of around 56%. These results revealed that the activity is improved by the preparation of the bimetallic CoMo and NiMo systems over the β-KIT-6 support. While the inclusion of Ni in the CoMo catalyst formulation decreased the activity considerably. Then, the relatively higher amounts of Ni in the trimetallic catalysts may cause the loss of CoMo or NiMo active sites in the sulfided samples.

The selectivity of the catalyst series is presented in Fig. 7. The selectivity calculated for the CoMo/β-KIT-6 for the production of biphenyl (DSD) was ~87%, while for cyclohexylbenzene was ~13% (HYD). Bicyclohexane and cracking products such as benzene, cyclohexane, and cyclohexenes were not detected. In the NiMo/β-KIT-6 catalysts, the HYD selectivity pathway was higher (25%) than in the CoMo/β-KIT-6 sample which is a typical result for a NiMo system. As expected, for the (0.6)NiCoMo/β-KIT-6 catalyst we observed that the incorporation of 0.6 Ni wt.% induced a clear increase in the hydrogenation route until 19%. However, a further increase of the Ni content resulted in a decrease of the HYD selectivity to 13% and 9% for the 1.2NiCoMo/β-KIT-6 and 2.4NiCoMo/β-KIT-6 catalysts, respectively. As mentioned below the excess of Ni may induce the formation of segregated β-$CoMoO_4$ or β-$NiMoO_4$ oxide crystalline phases.

3.3.2 HRTEM

The HRTEM micrographs for the sulfided NiMo/β-KIT-6 and CoMo/β-KIT-6 catalysts are shown in Fig. 8. The general aspect of the MoS_2 slabs in both catalysts resulted very similar.

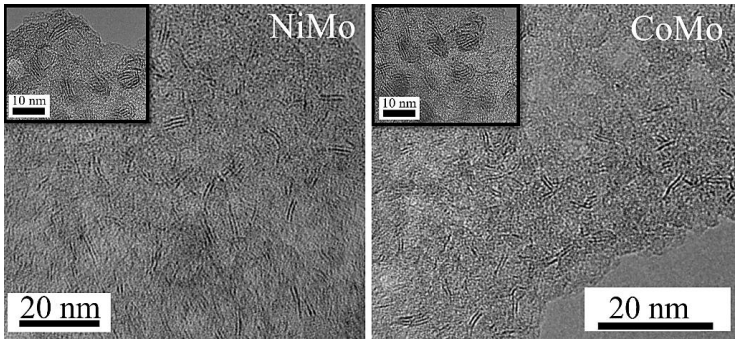

Fig. 8. The HRTEM images for the NiMo/β-KIT-6 and CoMo/β-KIT-6 sulfided catalysts. Inset. HRTEM micrographs from the pores partially filled with slabs.

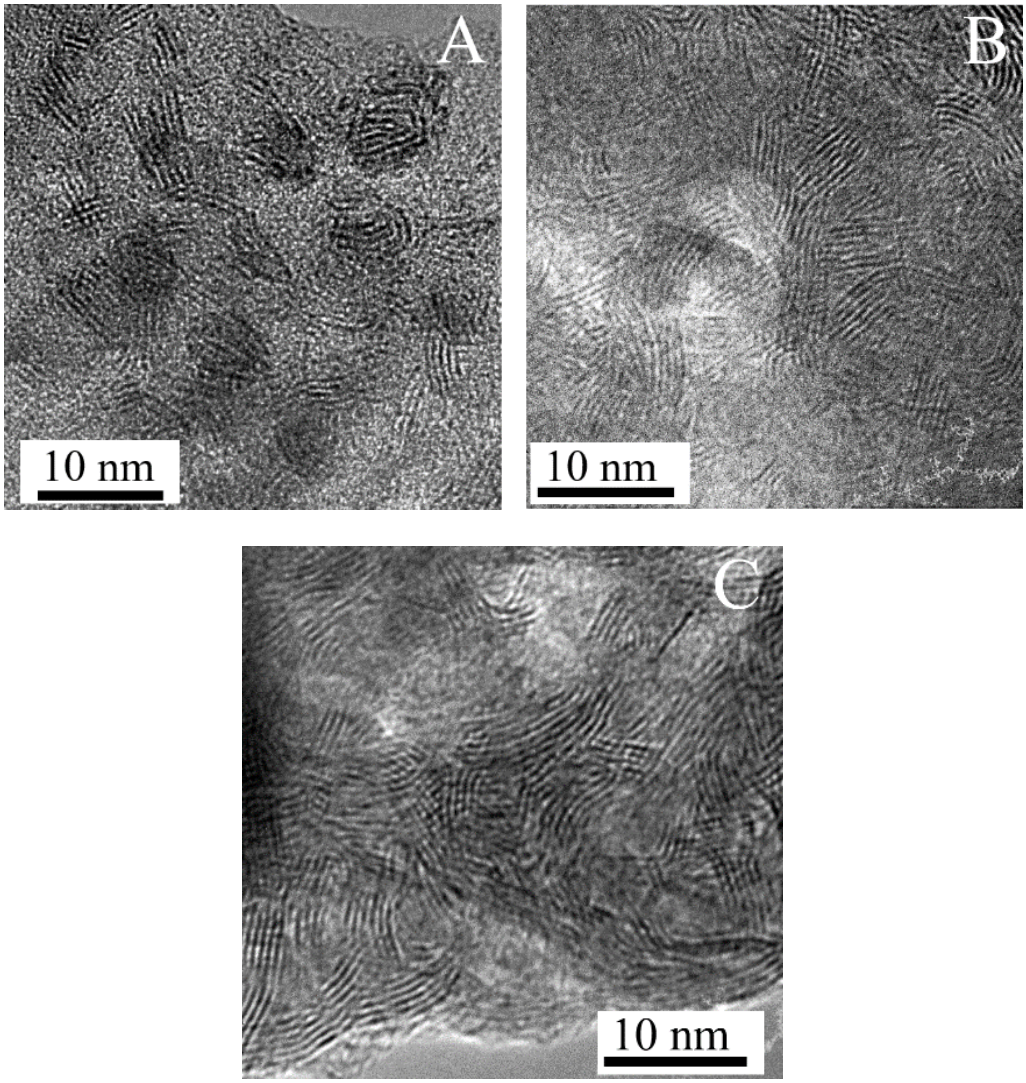

Fig. 9. The HRTEM images for the A)0.6NiCoMo/β-KIT-6, B)1.2NiCoMo/β-KIT-6 and C)2.4NiCoMo/β-KIT-6 sulfided catalysts.

Two different zones of the catalysts were observed, the first one showing no porosity and the second one showing MoS_2 slabs inside the pores. The length of the MoS_2 slabs was in the range between 3 to 5 nm which is in good agreement with the pore size distribution given in section 3.2.1. In the zones without pores, the active phase seems to be stacked preferably in clusters of two and three slabs for the NiMo catalyst, while in the CoMo sample it appears to be stacked in one and two slabs.

The micrographs for the trimetallic sulfide catalysts 0.6NiCoMo/β-KIT-6, 1.2NiCoMo/β-KIT-6 and 2.4NiCoMo/β-KIT-6 are shown in Fig. 9. It is possible to observe that the increase of the Ni concentration changes the morphology of the active phase entirely. For the 0.6NiCoMo/β-KIT-6, the slabs seem to be full-filling the pores, and the slabs appear to be curved. The curved slabs are associated with an increase in the hydrogenation pathway due to the increase in corner active sites (Nogueira *et al*., 2012). Our results agree with this model since we observed an increase in the hydrogenation route for this sample. In the case of the 1.2NiCoMo/β-KIT-6 and 2.4NiCoMo/β-KIT-6, the slabs have longer

lengths and higher stacking than in the previous case. So, the increase of Ni concentration in the trimetallic samples decreased the dispersion as suggested below.

The statistical analysis of the samples is given in Table 2. After the initial observation, the statistical analysis confirms clearly that the CoMo and NiMo catalysts have almost the same slab morphology. The average slab length ($\overline{L}$) resulted 3.7 and 3.9 nm for CoMo and NiMo catalysts, respectively. The average stacking number ($\overline{N}$) also resulted very similar i.e. 2.6 slabs per cluster for CoMo and 2.8 for NiMo. On the other hand, $\overline{L}$ and $\overline{N}$ for the trimetallic systems resulted larger than for the bimetallic systems in every case. The $\overline{L}$ value resulted 4.0, 5.3 and 8.7 for the 0.6NiCoMo/β-KIT-6, 1.2NiCoMo/β-KIT-6 and 2.4NiCoMo/β-KIT-6 sulfided catalysts respectively. The same behavior was obtained for the $\overline{N}$ parameter, starting with 3.3 slabs for 0.6NiCoMo/β-KIT-6, 4.7 slabs for 1.2NiCoMo/β-KIT-6 and 7.5 slabs for 2.4NiCoMo/β-KIT-6. These values obtained for the trimetallic catalysts seem to confirm the gradually loss of dispersion for the MoS_2 based active phase.

3.4 XPS

The Fig. 10 shows the Mo 3d (A), Co 2p (B) and Ni 2p (C) core level spectra obtained for the sulfided catalysts, respectively. The binding energies (BE) of the samples are shown in Table 3. It has to be noted that all samples only showed the S 2p peak at 162.0 eV (Koranyi *et al*., 1989), which is characteristic of S_2^- ions. The absence of the second component at a BE of around 168 eV characteristic of sulfate species (Siriwardane *et al*., 1990) indicates that the experimental procedure followed during sulfidation and sample transfer within the spectrometer chamber was efficient for avoiding air contact.

The BE value for the Mo $3d_{5/2}$ in all sulfided samples was 229.0 eV, which is similar to that typically reported for pure MoS_2 (Briggs *et al* (1990)). The absence of peaks related to the oxysulfide species (like $MoO_2S_2^{2-}$) indicates that a complete sulfidation of the molybdenum species has occurred. All sulfided samples have shown two Co 2p3/2 peaks at 778.9 eV and 781.9 ± 0.2 eV. The presence of the 779.9 eV signal could be related to the presence of the CoS_2 phase in agreement with our previous reports (Pawelec *et al*., 2008). The BE at 781.9 eV is assigned to the presence of Co ions that are not entirely sulfided (Tan *et al*., 1991). The $Ni2p_{3/2}$ peak in the Ni-containing samples also showed two XPS signals at 554.1 and 556.4 eV. The $Ni2p_{3/2}$ peak at 554.1 eV is associated with the presence of Ni sulfided species, while the BE at 556.4 eV is characteristic of Ni oxide surface species (Montesinos *et al*., 2008).

The surface atomic ratios between the different species were obtained and listed in Table 4.

Table 2. HRTEM statistical values for length and stacking of MoS_2 in the sulfided catalysts.

β-KIT-6	$\overline{L}$ (nm)		$\overline{N}$	
CoMo	3.7	±0.6	2.6	±0.7
NiMo	3.9	±0.7	2.8	±0.8
0.6NiCoMo	4.0	±0.5	3.3	±0.5
1.2NiCoMo	5.3	±0.6	4.7	±0.6
2.4NiCoMo	8.7	±1.4	7.5	±0.5

Table 3. Binding energies (eV) of the freshly sulfided catalysts.

β-KIT-6	$MO_3d_{5/2}$	$CO_2p_{3/2}$	$Ni2p_{3/2}$	S_2p
CoMo	229.0	778.8 (46) 782.1 (54)	-	162.0
0.6NiCoMo	229.0	778.9 (26)	854.1 (42)	162.0
1.2NiCoMo	229.0	781.9 (74) 778.8 (41) 781.7 (59)	856.6 (58) 854.1 (57) 856.4 (43)	162.0

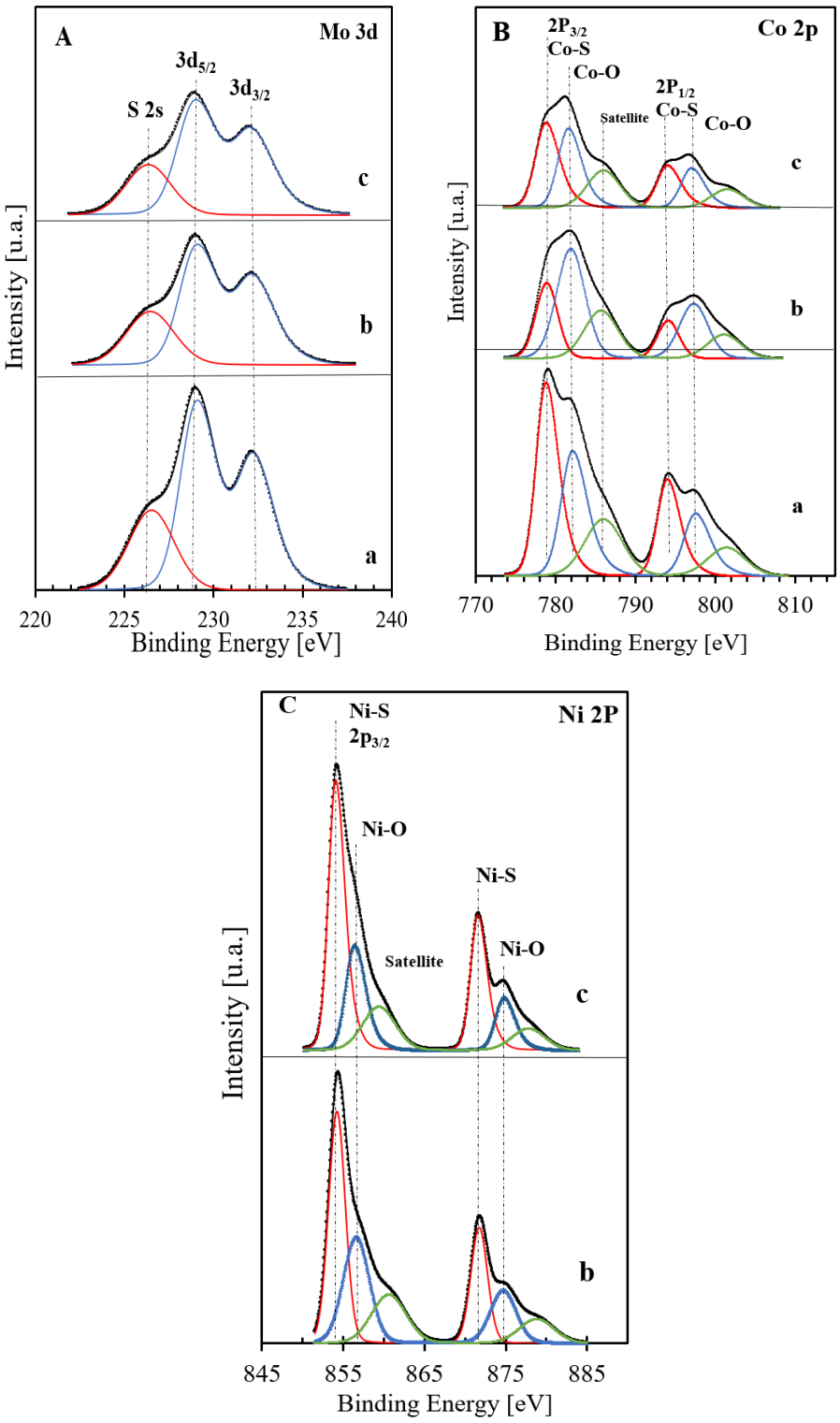

Fig. 10. XPS spectra for (x)NiCoMo/β-KIT-6 sulfided catalysts: A) Mo 3d and S 2s, B) Co 2p, C) Ni 2p and a)CoMo, b) 0.6NiCoMo and c) 1.2NiCoMo.

Table 4. Surface atomic ratios related to the sulfided catalysts

β-KIT-6	Mo/(Si+Al) at	Co/(Si+Al) at	Ni/(Si+Al) at
CoMo	0.053	0.013 (Sul.)	-
		0.015 (Oxi.)	
0.6NiCoMo	0.036	0.011 (Sul.)	0.004 (Oxi.)
		0.004 (Sul.)	0.005 (Oxi.)
1.2NiCoMo	0.027	0.008 (Sul.)	0.005(Oxi.)
		0.005 (Sul.)	0.003 (Oxi.)

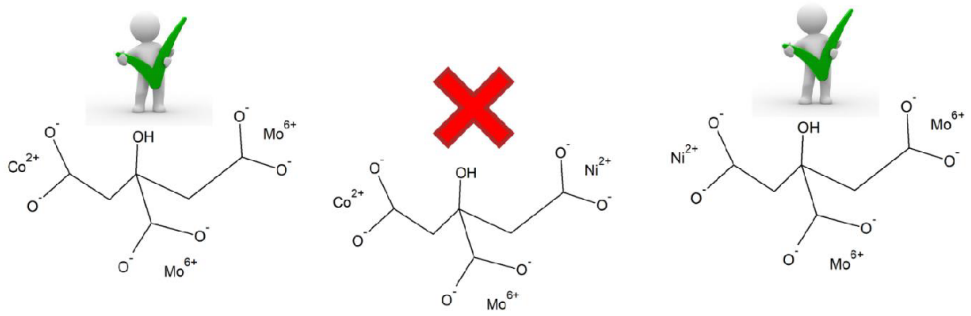

Scheme 1. Formation of the Mo-Co and Mo-Ni citrates under synthesis conditions but no in the trimetallic Ni-Co-Mo.

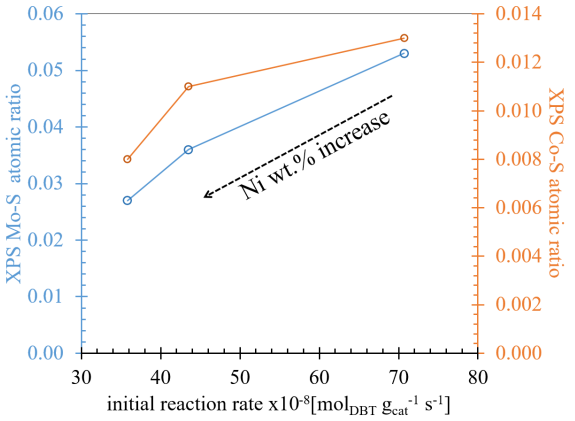

Fig. 11. Dependence between the surface sulfide Co and Mo species plotted as a function of the catalytic activity.

The highest value of the Mo/(Si+Al) surface atomic ratio was observed for the CoMo/β-KIT-6 sample. It was 1.5 and 2.0 times higher in comparison with the 0.6NiCoMo/β-KIT-6 and 1.2NiCoMo/β-KIT-6 samples, respectively. The cobalt surface atomic ratio was obtained considering both sulfide and oxide species. The sulfide Co species decreased linearly with the Ni wt% increment. Otherwise, the amount of oxide Co species is not linear with the Ni content. The surface sulfide Co species were 1.2 and 1.6 times higher in the sample CoMo/β-KIT-6, in comparison with the 0.6NiCoMo/β-KIT-6 and 1.2NiCoMo/β-KIT-6 samples, respectively. Finally, the surface sulfide Ni species were very similar in both Ni-containing samples, while the surface oxide Ni species decreased slightly when a higher quantity of nickel was incorporated (1.2 wt%). These results point out that nickel is segregated and does not participate in the promotion of the MoS_2 phase. Then, we propose a correlation between the surface sulfide Co and Mo species with the intrinsic catalytic activity as it is shown in Fig. 11.

As illustrated in Scheme 1, we propose that during the preparation of the trimetallic impregnation solution the Mo-Co and Mo-Ni citrate were formed as in the bimetallic catalysts, but not the trimetallic citrate. As XPS results suggested Ni remains excluded of the formation of the active sulfide phase, and it could be blocking the access to the CoMoS active sites. The formation of the $CoMoO_4$ crystalline phase observed by XRD support this assumption as well the catalytic activity results. Indeed, the hydrogenation function decreases with the increase in the Ni wt% content, which is unexpected for hydrotreating catalysts.

Also as a consequence of this mentioned blockage, the catalytic activity decreased considerably. Further characterization by TPD and Raman spectroscopy is in progress to fully understand this effect.

Conclusions

The KIT-6 support modified with zeolite beta synthesized in this study resulted with suitable textural properties for the preparation of HDS catalysts. The preparation of CoMo/β-KIT-6 and NiMo/β-KIT-6 over the support induced the highest catalytic activity among the series. As well, the β-KIT-6 support led to the highest activity when compared to SBA-15 or KIT-6 prepared HDS catalysts reported previously by our group. In the case of the trimetallic samples, we observed a clear decrease in the catalytic behavior with the addition of Ni to the system. Evidence obtained by HRTEM and XPS support the idea of Ni blocking the access of DBT to the CoMoS phase.

Acknowledgement

To SENER-CONACyT 117373 project for the financial support. To E. Aparicio and F. Ruiz for their expert technical assistance.

References

Abrokwah, R. Y., Deshmaneb, V. G., Kuilac D., (2016). Comparative performance of M-MCM-41 (M: Cu, Co, Ni, Pd, Zn and Sn) catalysts for steam reforming of methanol. *Journal of Molecular Catalysis A: Chemistry 425*, 10-20.

Alonso-Núñez, G., Bocarando, J., Huirache-Acuña, R., Álvarez-Contreras, L., Huang, Z.-D., Bensch, W., Berhault, G., Cruz, J., Zepeda, T.A., Fuentes, S., (2012). Influence of the activation atmosphere on the hydrodesulfurization of Co-Mo/SBA-15 catalysts prepared from sulfur-containing precursors. *Applied Catalysis A: General 419-420*, 95-101.

Briggs D., Seah M.P. (1990). *Practical Surface Analysis. Auger and X-ray Photoelectron Spectroscopy*, Wiley, New York/Salle and Sauerländer, p. 607.

Escobar, J., De Los Reyes, J. A., Ulín, C. A., Barrera, M. C., (2013). Highly active sulfided CoMo catalysts supported on $(ZrO_2\text{-}TiO_2)/Al_2O_3$ ternary oxides. *Materials Chemistry and Physics 143*, 213-222.

Gao, D., Duan, A., Zhang, X., Zhao, Z., E H., Li, J., Wang. H. (2015) .Synthesis of NiMo catalysts supported on mesoporous Al-SBA-15 with different morphologies and their catalytic performance of DBT HDS. *Applied Catalysis B: Environmental 165*, 269-284.

González-Cortés, S. L., Almegren, H. A., Kuznetsov, V. L., Qian, Y., Xiao, T., Edwards, P. P., (2015). Citric acid-assisted synthesis of γ-alumina-supported high loading CoMo sulfide catalysts for the hydrodesulfurization (HDS) and hydrodenitrogenation (HDN) reactions. *Applied Petrochemical Research 5*, 181-197.

Gonzalez-Cortes, S. L., Xiao, T. C., Lin, T. W., Green, M.L.H., (2006). Influence of double promotion on HDS catalysts prepared by urea-matrix combustion synthesis. *Applied Catalysis A: General 302*, 264-273.

Gotier, S., Tuel, A. (1995). Synthesis and characterization of Ti-containing mesoporous silicas. *Zeolites 15*, 601.

Guo, C., Wu, Y., Wang, X., Yang, B., (2013). Effect of the support calcination temperature on selective hydrodesulfurization of TiO_2 nanotubes supported CoMo catalysts. *Journal of Energy Chemistry 22*, 517-523.

Gutierrez, O. Y., Singh, S., Schachtl, E., Kim, J., Kondratieva, E., Hein, J., Lercher, J. A., (2014). *Effects of the Support on the Performance and Promotion of (Ni)MoS_2 Catalysts for Simultaneous Hydrodenitrogenation and Hydrodesulfurization*. ACS.

Gutiérrez-Tinoco, O., Romero-Moreno, K., Leocadio-Cerón, E., Fuentes-Zurita, G., Klimova-Berestneva, T., (2006). Soportes SBA-15 modificados con Ti y Zr por injertado químico para catalizadores NiMo de HDS profunda. *Revista Mexicana de Ingeniería Química 5*, 179-187.

He, F., Luo, J., Liu, S., (2016). Novel metal loaded KIT-6 catalysts and their applications in the catalytic combustion of chlorobenzene. *Chemical Engineering Journal 294*, 362-370.

Kaluž, L., Zdražil, M., Vít, Z., Gulková, D., (2012). $CoMo/ZrO_2$ Hydrodesulfurization catalysts prepared by chelating agent assisted spreading. *Procedia Engineering 42*, 261-266.

Kim, T.-W., Kleitz, F., Paul, B., Ryoo, R. (2005). MCM-48-like large mesoporous silicas with tailored pore structure: Facile synthesis domain in a ternary triblock copolymer-butanol-water system. *Journal American Chemical Society 127*, 7601.

Koranyi, T.I., Manninger, I., Paal, Z., Marks, O., Gunter, J.R., (1989). Activation of unsupported CoMo catalysts in thiophene hydrodesulfurization. *Journal of Catalysis 116*, 422-439.

Montesinos, A., Zepeda, T. A., (2008). High hydrogenation performance of the mesoporous NiMo/Al(Ti, Zr)-HMS catalysts. *Microporous and Mesoporous Materials 113*, 146-162.

Munguía-Guillén, J.L., Vernon-Carter, E.J., De los Reyes-Heredia, J.A., Viveros-García, T., (2016). Efecto del tensoactivo en la síntesis de catalizadores $CoMo/Al_2O_3$ obtenidos por microemulsión inversa para la hidrodesulfuración de dibenzotiofeno. *Revista Mexicana de Ingeniería Química 15*, 893-902.

Nogueira, A., znaiguia, R., Uzio, D., Afanasiev, Berhault, P. G. (2012). Curved nanostructures of unsupported and Al_2O_3-supported MoS_2 catalysts: Synthesis and HDS catalytic properties. *Applied Catalysis A: General 429-430*, 92-105.

Olguin, E., Vrinat, M., Cedeño, L., Ramirez, J., Borque, M., López-Agudo, A., (1997). The use of TiO_2-Al_2O_3 binary oxides as supports for Mo-based catalysts in hydrodesulfurization of thiophene and dibenzothiophene. *Applied Catalysis A: General 165*, 1-13.

Pawelec, B., Castaño P. and Zepeda, T. A. (2008). Morphological investigation of nanostructured CoMo catalysts. *Applied Surface Science 254*, 4092-4102.

Pratt, K. C., Sanders, J. V., Christov, V., (1990). Morphology and activity of MoS_2 on various supports: Genesis of the active phase. *Journal of Catalysis 124*, 416-432.

Ramirez, J., Ruiz-Ramirez, L., Cedeno, L., Harle, V., Vrinat, M., Breysse. M., (1993). Titania-alumina mixed oxides as supports for molybdenum hydrotreating catalysts. *Applied Catalysis A: General 93*, 163-180.

Reddy, B. M., Chowdhury, B., Smirniotis, P. G., (2001). An XPS study of La_2O_3 and IN_2O_3 influence on the physicochemical properties of MoO_3/TiO_2 catalysts. *Applied Catalysis A: General 211*, 19-30.

Rezaei, M. Chermahini, A. N. Dabbagh, H. A. (2017). Green and selective oxidation of cyclohexane over vanadium pyrophosphate supported on mesoporous KIT-6. *Chemical Engineering Journal 314*, 515-525.

Siriwardane R. V. and Poston, J.A. (1990). Interaction of H_2S with zinc titanate in the presence of H_2 and CO. *Applied Surface Science 45*, 131-139.

Song, C., Ma, X. (2003). New design approaches to ultra-clean diesel fuels by deep desulfurization and deep dearomatization. *Applied Catalysis B: Environmental 41*, 207-238.

Souza, M. J.B., Garrido-Pedrosa, A. M., Cecilia, J.A., Gil-Mora, A.M., Rodríguez-Castellón, E. (2015). Hydrodesulfurization of dibenzothiophene over PtMo/MCM-48 catalysts. *Catalysis Communication 69*, 217-222.

Suresh, C., Pérez Cabrera, L., Aliaga, J.A, Díaz de León, J.N., Zepeda, T.A., Fuentes, S., Berhault, G., Alonso-Núñez, G., (2017). Formation of co-promoted MoS_2 fullerene-like nanostructures on SBA-15 as effective hydrodesulfurization catalyst. *Catalysis Letters 147*, 46-57.

Suresh, C., Pérez-Cabrera, L., Díaz de León, J.N., Zepeda, T.A., Alonso-Núñez, G., Fuentes Moyado, S., (2017). Highly active CoMo/Al (10) KIT-6 catalysts for HDS of DBT: Role of structure and aluminum heteroatom in the support matrix. *Catalysis Today 296*, 214-218.

Tan, B.J. Klabunde, K.J., Sherwood P.M.A., (1991). XPS studies of solvated metal atom dispersed (SMAD) catalysts. Evidence for layered cobalt-manganese particles on alumina and silica. *Journal of the American Chemical Society 113*, 855-861.

Tavizón-Pozos, J. A., Suárez-Toriello, V. A., de los Reyes, J. A., Guevara-Lara, A., Pawelec, B., G. Fierro, J. L., Vrinat, M., Geantet, C., (2016). Deep hydrodesulfurization of dibenzothiophenes over NiW sulfide catalysts supported on sol-gel titania-alumina. *Topics in Catalysis 59*, 241-251.

Thommes, M., Kaneko, K., Neimark, A. V., Olivier, J. P., Rodriguez-Reinoso, F., Rouquerol, J., Sing, K. S. W., (2015). Physisorption of gases, with special reference to the evaluation of surface area and pore size distribution (IUPAC Technical Report). *Pure and Applied Chemistry*, 1051-1069.

Topsoe, H., Clausen, B.S., Massoth, F.E., (1996). *Hydrotreating Catalysis: Science and Technology*, Springer, Berlin,.

Trejo, F., Rana, Mohan S., Ancheyta, J., (2008). CoMo/MgO-Al_2O_3 supported catalysts: An alternative approach to prepare HDS catalysts. *Catalysis Today 130*, 327-336.

Wei, S., He, H., Cheng, Y., Yang, C., Zeng, G., Kang, L., Qian, H., Zhu, C., (2017) Preparation, characterization, and catalytic performances of cobalt catalysts supported on KIT-6 silicas in oxidative desulfurization of dibenzothiophene. *Fuel 200*, 11-21.

Zepeda, T.A., Díaz de León, J.N., Fuentes, S., Alonso-Núñez, G., Torres-Otañez G., and Pawelec, B., (2014). Hydrodesulfurization enhancement of heavy and light S-hydrocarbons on NiMo/HMS catalysts modified with Al and P. *Applied Catalysis A: Gen. 484*, 108-121.

Zepeda, T. A., Fierro, J. L. G., Pawelec, B., Nava, R., Klimova, T., Fuentes, G. A., Halachev. T. (2005). Synthesis and characterization of Ti-HMS and CoMo/Ti-HMS oxide materials with varying Ti content. *Chemical Materials 17*, 4062-4073.

Zhang, D., Duan, A., Zhao, Z., Xu, C., (2010). Synthesis, characterization, and catalytic performance of NiMo catalysts supported on hierarchically porous Beta-KIT-6 material in the hydrodesulfurization of dibenzothiophene. *Journal of Catalysis 274*, 273-286.

Zhang, D., Duan, A., Zhao, Z., Xu, C., (2010). Synthesis, characterization, and catalytic performance of NiMo catalysts supported on hierarchically porous Beta-KIT-6 material in the hydrodesulfurization of dibenzothiophene. *Journal of Catalysis 274*, 273-286.